Three-Dimensional Spherical-Shaped UPML for FDTD with Cubic Lattices

Lu Wang [1], Mengjun Wang [1], Kanglong Zhang [1], Wenjie Cui [1], Hongxing Zheng [1*], and Erping Li [2]

[1] School of Electronics and Information Engineering
Hebei University of Technology, Tianjin, TJ 22, China
wanglu_william@163.com, wangmengjun@hebut.edu.cn, zhangkanglong@yeah.net, wjcui_driver@163.com,
*hxzheng@ hebut.edu.cn

[2] University of Illinois at Urbana-Champaign Institute
Zhejiang University, Haining, ZJ 573, China
liep@zju.edu.cn

Abstract ─ Spherical-shaped uniaxial perfectly matched layer (SS-UPML), an absorbing boundary for three-dimensional (3-D) finite-difference time-domain (FDTD) method with cubic cells, is proposed and applied to different objects. This boundary is used for truncating the computational domain to absorb outgoing electromagnetic waves, which has the advantages of higher efficiency and accuracy, compared with the conventional UPML. Update equations are transformed by coordinate rotation to better fit the Cartesian system. Different numerical experiments are implemented to verify the stability and practicability of the proposed boundary in 3-D case. Obtained results illustrate that about a half grid and computational time can be saved after SS-UPML is used, which is the foundation of a wider range of applications.

Index Terms ─ FDTD, Cartesian coordinate system, spherical boundary truncation, three-dimension, UPML.

I. INTRODUCTION

The finite-difference time-domain (FDTD) method is one of the most effective ideas in calculating radiation problems of electromagnetic waves, and has rapidly developed since it was introduced by Yee [1]. Finite computer memory, however, cannot meet the requirement of infinite problems. Thus, highly efficient absorbing boundary condition plays an important role in simulation. Uniaxial perfectly matched layer (UPML), a valid way for truncation without reflected wave, seems like a lossy media wall that surrounds the computing space. Sacks and Gedney described this method from the respect of uniaxial media with conductivity permeability and permittivity tensors [2], [3], and Chew implemented a similar one from another respect of Maxwell update equations with complex coordinate stretching along three directions in the Cartesian system [4]. In fact, the essence of these two derivations are the same, but reveal the different characteristics of UPML. On the other hand, it avoids the nonphysical field splitting caused by Bérenger's PML, which was proposed and investigated in [5]-[9], whereas has the equally impressive In this paper, a spherical-shaped UPML (SS-UPML) strategy is discussed for FDTD in three-dimensional (3-D) condition. We establish the SS-UPML in the Cartesian coordinate system with cubic cells, as shown in Fig. 1. A continuous spherical-shaped boundary is used to truncate free space. After discretizing it, a two-dimensional section is obtained and placed on the right, which visibly avoids calculating unnecessary grids at corners and edges, and can absorbs outgoing wave perfectly. The practicability and efficiency of the method are verified by simulating different radiation samples, and are compared with the conventional UPML. The results indicate that the proposed method obviously reduce the computational memory and time, and maintain at the same error level with the original UPML.

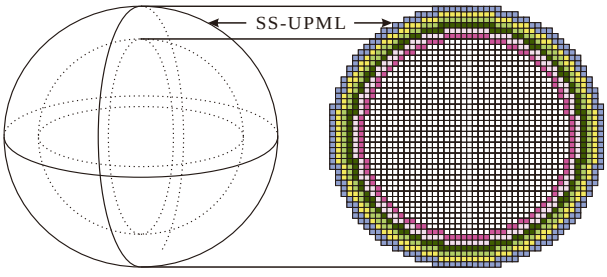

Fig. 1. SS-UPML in Cartesian coordinate system.

In Section II, we describe two advantages of this approach, *obvious reduction of memory and smaller incident angle*, that are the basis of successful application. Section III introduces the fundamental formulations of 3-D SS-UPML. Lastly, in Section IV, several numerical experiments are implemented to verify the performance

Submitted On: October 22, 2018
Accepted On: December 14, 2018

of our method.

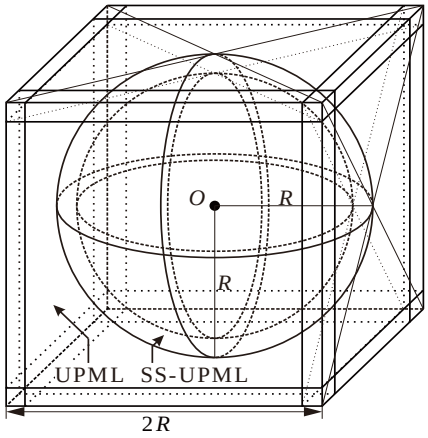

Fig. 2. Illustration of SS-UPML and UPML.

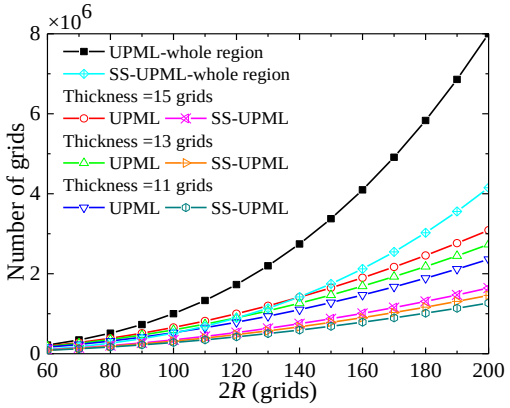

Fig. 3. The number of grids varies with R and thickness in two boundaries.

II. THREE-DIMENSIONAL SS-UPML

We are intending to introduce the features of 3-D SS-UPML, from which are where it differs the traditional methods. Pursuant to the previous description, we know that this boundary has less computer memory requirements than traditional methods; here we will carry out a quantitative analysis. Besides, it has another advantage of smaller incident angle, compared to the same source point in a cubic region. More details are given in the following.

A. Fewer computational memory

In order to clearly demonstrate the difference between the conventional cubic UPML and SS-UPML, we establish them with the size of $2R$ and the radius of R, respectively, and with a same centroid, as shown in Fig. 2. The thickness of these two boundaries is equal, thus, they are tangent at inside and outside.

It is clear that the volume of SS-UPML truncated region is $(4/3)\pi R^3$, and of UPML is $(2R)^3$, almost doubled to the former. This implies the FDTD cubic cells with two boundaries may have the same relationship in quantity.

After dispersing these two regions in Cartesian coordinate system, the cubic UPML region is divided into a number of congruent cube-meshes. The curved SS-UPML boundary needs to approximate by groups of staircase lattices following the conformal condition [19]. Therefore, we can count the number of grids in both regions easily. The statistics of variations with different thickness and R (both units are grids, in order to illustrate the difference in the respect of quantity, and it has nothing to do with the size) are shown in Fig. 3. Apparently, an increasing number of grids are saved due to the use of our boundary with the edge length growth. Besides, the number of grids in SS-UPML region has always been about half of the UPML in not only the whole regions, but also the absorbers.

In our FDTD programs, the parameters of lattice are recorded by different variables, which means the computational memory will go forth and multiplying as the radius increases. On the other hand, the parameters of boundary are more complicated than free space, so it needs more memory to store and more time to calculate. Thus, fewer grids in both regions leads to considerable decline of memory in executing the programs. Further, this will bring the possibility to reduces computing time and enhance its efficiency.

B. Smaller incident angle

To plainly compare the difference of the incident angle of the same incident wave between SS-UPML and UPML, we define two computational regions, as we did in the last part. As clearly shown in Fig. 4, the point $O(x_0, y_0, z_0)$ is the geometric center of both region, the wave source is placed at an arbitrary point $S(x_s, y_s, z_s)$ in the region, and point $S'(x_s', y_s', z_s')$ is the projection of S on the right side of cubic region. After that, the wave will spread all around and eventually propagate to the interface of free space and absorption layer. For a more intuitive explanation of the relationship between the two, we assume that the wave propagates only to the right and the incident point is $P(x_p, y_p, z_p)$, which is on the right side of the region. The angle θ in the Fig. 4 is the angle of incidence on the boundary. According to the assumption above, the expressions of θ in different regions can be obtained by using the triangular relationship:

$$\theta_{\text{sph}} = \arccos\left(\frac{dis^2 - (x_s - x_0)^2 - (y_s - y_0)^2 - (z_s - z_0)^2 + R^2}{2R \cdot dis}\right), \tag{1}$$

$$\theta_{\text{cub}} = \arccos\left(\frac{dis^2 - (x_{s'} - x_p)^2 - (z_{s'} - z_p)^2 + (y_s - y_{s'})^2}{2(y_s - y_{s'}) \cdot dis}\right), \tag{2}$$

where dis represents the distance between point S and P, and can be expressed as:

$$dis = \sqrt{(x_s - x_p)^2 + (y_s - y_p)^2 + (z_s - z_p)^2}\ . \tag{3}$$

Now, we consider a special case, that is point S

coinciding with point *O*. Obviously, the wave propagates along the radius in the spherical region, which means that it always perpendicular to the boundary. In the square region, however, normal incidence can only be achieved when *P* is at the center of the right side, and the angle will become large when it is close to the border. This significant different trend is shown in Fig. 5. On the other hand, we mostly place the scatter at the center, which means the wave will always propagate from the region near the centroid, and have the similar incident angle pattern as mentioned. This feature is very helpful for improving calculation accuracy and reducing errors, which will be verified below.

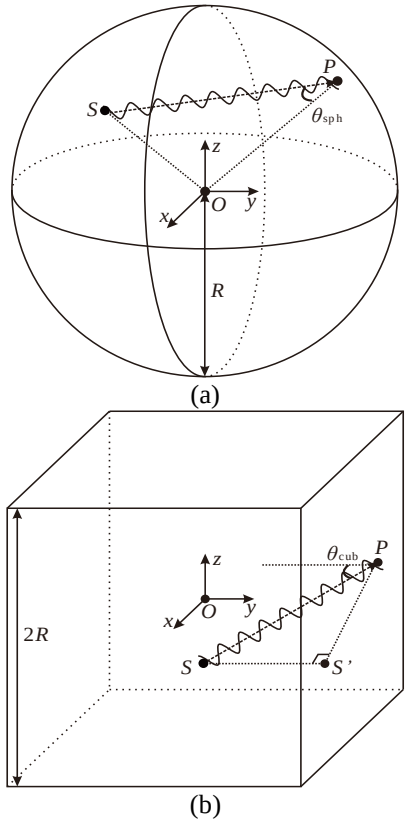

Fig. 4. Wave propagation in: (a) SS-UPML and (b) UPML.

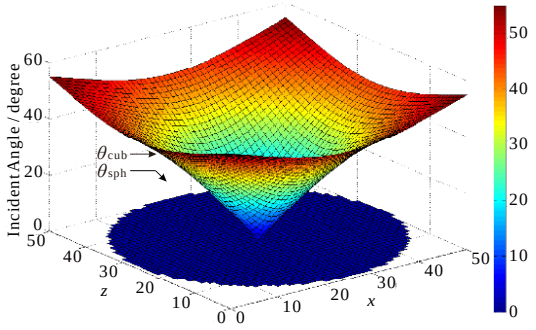

Fig. 5. Comparison of incident angle between two boundaries.

III. FORMULATIONS

The UPML, a physical model based on anisotropic perfectly matched medium, is one of the excellent absorbing boundaries of the FDTD method. It is derived from Maxwell equations with uniaxial media tensors, and does not have to split the field into sub-components. Therefore, it can calculate more complicated objects with different materials and structures. We use $\bar{\bar{\varepsilon}}$ and $\bar{\bar{\mu}}$ diagonal matrix to represent the electric and magnetic permittivity tensor in absorbing region, respectively. These two parameters should meet the requirement of matching conditions, which are $\bar{\bar{\varepsilon}} = \varepsilon_u \bar{\bar{s}}$ and $\bar{\bar{\mu}} = \mu_u \bar{\bar{s}}$, where ε_u and μ_u are the relatively permittivity and permeability of the absorber, respectively, and $\bar{\bar{s}}$ is matching matrix, to ensure that the impedance of the medium and the free space are the same. Inserting them into Ampere and Faraday law, we have:

$$\nabla \times \boldsymbol{H} = j\omega\varepsilon_u \bar{\bar{s}} \boldsymbol{E}\ ,\ \nabla \times \boldsymbol{E} = -j\omega\mu_u \bar{\bar{s}} \boldsymbol{H}\ . \tag{4}$$

The matrix $\bar{\bar{s}}$ has different expressions for different directions. For example, if the interface is perpendicular to *x*-axis, it can be written as $\bar{\bar{s}}_x = \mathrm{diag}[s_x^{-1}, s_x, s_x]$, where $s_x = \kappa_x + \sigma_x / j\omega\varepsilon_0$, so does $\bar{\bar{s}}_y$ and $\bar{\bar{s}}_z$. Inside the spherical boundary, it is obvious that the interface is perpendicular to the radius. Therefore, we should set the matching matrix as the product of $\bar{\bar{s}}_x$, $\bar{\bar{s}}_y$ and $\bar{\bar{s}}_z$ to achieve the same purpose, which can be expressed as:

$$\bar{\bar{\varsigma}} = \varsigma_u \bar{\bar{s}}_x \cdot \bar{\bar{s}}_y \cdot \bar{\bar{s}}_z = \varsigma_u \cdot \mathrm{diag}[s_x^{-1} s_y s_z, s_x s_y^{-1} s_z, s_x s_y s_z^{-1}], \tag{5}$$

where ς represents ε or μ. Directly inserting (5) into (4) and transforming them into time domain will lead to a convolution between coefficients and ***E***-field, which are not advisable, since implementing it would be computationally intensive. A more efficient approach is to define a proper constitutive relationship to decouple the frequency-dependent terms as follow:

$$D_x = \varepsilon(s_z/s_x)\cdot E_x,\ D_y = \varepsilon(s_x/s_y)\cdot E_y,\ D_z = \varepsilon(s_y/s_z)\cdot E_z. \tag{6}$$

After simplify these relations, we obtain a two-step update cycle likes ***D-E-B-H-D***. Obviously, it is more complicated than the standard FDTD time domain update equations, and costs more computational time and memory. While, we can use radial subcomponents in SS-UPML to overcome this defect, which is expressed by using subscript '*r*' in the following. Therefore, (4) can be transformed into time domain and rewritten as:

$$\kappa_r \frac{\partial D_{xr}}{\partial t} + \frac{\sigma_r}{\varepsilon_0} D_{xr} = \frac{\partial H_{zr}}{\partial y} - \frac{\partial H_{yr}}{\partial z}, \tag{7a}$$

$$\kappa_r \frac{\partial D_{yr}}{\partial t} + \frac{\sigma_r}{\varepsilon_0} D_{yr} = \frac{\partial H_{xr}}{\partial z} - \frac{\partial H_{zr}}{\partial x}, \tag{7b}$$

$$\kappa_r \frac{\partial D_{zr}}{\partial t} + \frac{\sigma_r}{\varepsilon_0} D_{zr} = \frac{\partial H_{yr}}{\partial x} - \frac{\partial H_{xr}}{\partial y}, \tag{7c}$$

$$-\kappa_r \frac{\partial B_{xr}}{\partial t} - \frac{\sigma_r}{\varepsilon_0} B_{xr} = \frac{\partial E_{zr}}{\partial y} - \frac{\partial E_{yr}}{\partial z}, \tag{8a}$$

$$-\kappa_r \frac{\partial B_{yr}}{\partial t} - \frac{\sigma_r}{\varepsilon_0} B_{zr} = \frac{\partial E_{xr}}{\partial z} - \frac{\partial E_{zr}}{\partial x}, \tag{8b}$$

$$-\kappa_r \frac{\partial B_{zr}}{\partial t} - \frac{\sigma_r}{\varepsilon_0} B_{zr} = \frac{\partial E_{yr}}{\partial x} - \frac{\partial E_{xr}}{\partial y}. \tag{8c}$$

In order to make these equations to better fit the Cartesian coordinates, resolution of these variables in each direction is needed. We should decompose each radial component along x-, y- and z-axis through the rotation relationship, and then calculate them according to the relative position. Fortunately, this method can also overcome the problem of different update coefficient forms caused by different permittivity and permeability between free space and absorbing region. Therefore, we can obtain uniform equations throughout the entire computational region, which ensure the global consistency of updating and highly efficient of programing.

In 3-D condition, the angle between the wave vector $\boldsymbol{r}$ and the z-axis is θ, and the angle between $\boldsymbol{r}$ and the x-axis is φ. Thus, each radial component's position can be identified, and its update equations (7) and (8) can be rewritten as:

$$D_{xr}\big|_{\xi+1/2,\psi,\gamma}^{n+1} = CA\cdot D_{xr}\big|_{\xi+1/2,\psi,\gamma}^{n} + CB\cdot(H_{zr}\big|_{\xi+1/2,\psi+1/2,\gamma}^{n+1/2} - H_{zr}\big|_{\xi+1/2,\psi-1/2,\gamma}^{n+1/2} - H_{yr}\big|_{\xi+1/2,\psi,\gamma+1/2}^{n+1/2} + H_{yr}\big|_{\xi+1/2,\psi,\gamma-1/2}^{n+1/2}), \tag{9a}$$

$$D_{yr}\big|_{\xi,\psi+1/2,\gamma}^{n+1} = CA\cdot D_{yr}\big|_{\xi,\psi+1/2,\gamma}^{n} + CB\cdot(H_{xr}\big|_{\xi,\psi+1/2,\gamma+1/2}^{n+1/2} - H_{xr}\big|_{\xi,\psi+1/2,\gamma-1/2}^{n+1/2} - H_{zr}\big|_{\xi+1/2,\psi+1/2,\gamma}^{n+1/2} + H_{zr}\big|_{\xi-1/2,\psi+1/2,\gamma}^{n+1/2}), \tag{9b}$$

$$D_{zr}\big|_{\xi,\psi,\gamma+1/2}^{n+1} = CA\cdot D_{zr}\big|_{\xi,\psi,\gamma+1/2}^{n} + CB\cdot(H_{yr}\big|_{\xi+1/2,\psi,\gamma+1/2}^{n+1/2} - H_{yr}\big|_{\xi-1/2,\psi,\gamma+1/2}^{n+1/2} - H_{xr}\big|_{\xi,\psi+1/2,\gamma+1/2}^{n+1/2} + H_{xr}\big|_{\xi,\psi-1/2,\gamma+1/2}^{n+1/2}), \tag{9c}$$

$$B_{xr}\big|_{\xi,\psi+1/2,\gamma+1/2}^{n+3/2} = CA\cdot B_{xr}\big|_{\xi,\psi+1/2,\gamma+1/2}^{n+1/2} - CB\cdot(E_{zr}\big|_{\xi,\psi+1,\gamma+1/2}^{n+1} - E_{zr}\big|_{\xi,\psi,\gamma+1/2}^{n+1} - E_{yr}\big|_{\xi,\psi+1/2,\gamma+1}^{n+1} + E_{yr}\big|_{\xi,\psi+1/2,\gamma}^{n+1}), \tag{10a}$$

$$B_{yr}\big|_{\xi+1/2,\psi,\gamma+1/2}^{n+3/2} = CA\cdot B_{yr}\big|_{\xi+1/2,\psi,\gamma+1/2}^{n+1/2} - CB\cdot(E_{xr}\big|_{\xi+1/2,\psi,\gamma+1}^{n+1} - E_{xr}\big|_{\xi+1/2,\psi,\gamma}^{n+1} - E_{zr}\big|_{\xi+1,\psi,\gamma+1/2}^{n+1} + E_{zr}\big|_{\xi,\psi,\gamma+1/2}^{n+1}), \tag{10b}$$

$$B_{zr}\big|_{\xi+1/2,\psi+1/2,\gamma}^{n+3/2} = CA\cdot B_{zr}\big|_{\xi+1/2,\psi+1/2,\gamma}^{n+1/2} - CB\cdot(E_{yr}\big|_{\xi+1,\psi+1/2,\gamma}^{n+1} - E_{yr}\big|_{\xi,\psi+1/2,\gamma}^{n+1} - E_{xr}\big|_{\xi+1/2,\psi+1,\gamma}^{n+1} + E_{xr}\big|_{\xi+1/2,\psi,\gamma}^{n+1}), \tag{10c}$$

where

$$\begin{cases} \xi = r\sin\theta\cos\varphi \\ \psi = r\sin\theta\sin\varphi \\ \gamma = r\cos\theta \end{cases}, \tag{11}$$

are the transform relationship between the Cartesian and spherical coordinate system, and

$$CA = \frac{2\varepsilon_u\varepsilon_0\kappa_r - \sigma_r\Delta t}{2\varepsilon_u\varepsilon_0\kappa_r + \sigma_r\Delta t},\ CB = \frac{2\varepsilon_u\varepsilon_0\Delta t}{(2\varepsilon_u\varepsilon_0\kappa_r + \sigma_r\Delta t)\delta}, \tag{12}$$

where δ is the size of cubic grids. Moreover, the feature is the same in ***D*-*E*** and ***B*-*D*** relationships:

$$E_{xr}\big|_{\xi+1/2,\psi,\gamma}^{n+1} = CA\cdot E_{xr}\big|_{\xi+1/2,\psi,\gamma}^{n} + CE\cdot(CP\cdot D_{xr}\big|_{\xi+1/2,\psi,\gamma}^{n+1} - CQ\cdot D_{xr}\big|_{\xi+1/2,\psi,\gamma}^{n}), \tag{13}$$

$$H_{xr}\big|_{\xi,\psi+1/2,\gamma+1/2}^{n+3/2} = CA\cdot H_{xr}\big|_{\xi,\psi+1/2,\gamma+1/2}^{n+1/2} + CF\cdot(CP\cdot B_{xr}\big|_{\xi,\psi+1/2,\gamma+1/2}^{n+3/2} - CQ\cdot B_{xr}\big|_{\xi,\psi+1/2,\gamma+1/2}^{n+1/2}), \tag{14}$$

where

$$CE = \frac{1}{(2\varepsilon_0\kappa_r + \sigma_r\Delta t)\varepsilon_u\varepsilon_0}, CF = \frac{1}{(2\varepsilon_0\kappa_r + \sigma_r\Delta t)\mu_u\mu_0},$$
$$CP = 2\varepsilon_u\varepsilon_0\kappa_r + \sigma_r\Delta t, CQ = 2\varepsilon_u\varepsilon_0\kappa_r - \sigma_r\Delta t. \tag{15}$$

Here, we only list the x-component as an example to illustrate the update process; the other two have similar forms of calculation. The two key parameters, σ_r and κ_r, are important factors to the absorption effect, which can be set by using a polynomial variation grading of the loss with depth of ρ in SS-UPML:

$$\sigma_r(\rho) = -\left(\frac{\rho}{\chi}\right)^m \frac{(m+1)\ln(R_0)}{2\eta_0\rho}, \tag{16}$$

$$\kappa_r(\rho) = 1 + (\kappa_{r\max} - 1)\cdot(\rho/\chi)^m, \tag{17}$$

where χ is the thickness of the SS-UPML, R_0 represents the desired reflection error which should be specified before computation, η_0 is wave impedance in free space, $\kappa_{r\max}$ is an integer whose increase will result in an increase in the level of attenuation, and m determines the speed of parameter growth. A large m yields a σ_r distribution that is relatively flat near the SS-UPML surface. However, deeper within the boundary, σ_r increases more rapidly than for small m. In this way, σ_r increases from 0 at ξ = 0, the inner surface of the absorber, to the maximum value at $\xi = \gamma$, the outside of the boundary. Similarly, κ_r increases from 1 to $\kappa_{r\max}$ at the same position. After finishing these preparations, different numerical experiments are implemented to verify its performance.

IV. NUMERICAL EXPERIMENTS

We have implemented several numerical experiments to verify the stability, accuracy and efficiency of the proposed SS-UPML with 3-D FDTD cubic lattice codes. The calculating process is shown as follow.

A. Dipole source excitation in spherical-shell

The proposed method is built in the Cartesian coordinate system, so the spherical-shaped boundary is

approximated by a series of cubic latticework, whose profile looks like staircase. In order to verify the stability of the SS-UPML, which is the most important performance for absorbing boundary, we excite a source in a spherical-shell-shaped region. It means that in traditional calculation space, we use SS-UPML to truncate the outer boundary, so the computational space becomes spherical. Then we define an anti-SS-UPML ball, which has identical parameters with truncated boundary, whereas the value increasing direction is from the outer to the inner. After we put this ball in the middle of the calculation area, the shape of free space will like a spherical-shell, with two absorbing regions on both sides. As comparison, we define a similar region surrounded by conventional UPML and a same inner ball in the middle, as shown in Fig. 6. There is one thing to be aware of is that the position of dipole is equivalent at anywhere inside the SS-UPML, because of the perfect symmetry of the region, whereas it is not in the cubic region. Therefore, we should place the dipole at different positions to compare the quality of the two.

In this simulation, we choose three representative positions as examples in cubic region, which are on the lower, lower left and upper left rear directions, corresponding to point *A*, *B* and *C*, respectively. In spherical region, these three points can be marked at the same position by converting (r, θ, φ) into (x, y, z) coordinates. The dimension of the cubic computational domain is set as 201×201×201, which means there are 8.12 million grids in total. After truncated by SS-UPML with diameter 201 grids, however, the total number of mesh that need to be calculated are reduced to 4.15 million, which means that it saves 48.8% of memory, consistent with the previous predictions. The radius of the inner anti-SS-UPML ball is 20 grids. The positions of point *A*, *B*, and *C* are (0, 0, -55), (0, -50, -50), and (-40, -40, 40), and the view points of them are (0, 0, -45), (0, -40, -40), and (-30, -30, 30), respectively. Moreover, 15 layers of absorber are used to absorb the outgoing wave in both two cases. The edge length of the cubic cell is 5cm, and the time step is 83.33ps. We set the program to run 10000 steps, which is a long enough time to test its stability. The dipole is placed parallel to the *z*-axis at three points, whose radiation field in free space in time domain can be expressed as:

$$\boldsymbol{E}(\boldsymbol{r},t)=\frac{\mu_0}{4\pi r}\left\{\boldsymbol{e}_r\left[\frac{c_0}{r}\frac{\partial}{\partial t}+\left(\frac{c_0}{r}\right)^2\right]2\cos\theta+\boldsymbol{e}_\theta\left[\frac{\partial^2}{\partial t^2}+\frac{c_0}{r}\frac{\partial}{\partial t}+\left(\frac{c_0}{r}\right)^2\right]\sin\theta\right\}p\left(t-\frac{r}{c_0}\right), \quad (18)$$

where, c_0 is the speed of light in vacuum, r is the distance between dipole and view point. It is clearly that the electric field is only related to the angle and distance, due to the pose of dipole. In this sample, we use Gaussian pulse as an excitation, which is expressed as:

$$p(t)=10^{-10}e^{-[(t-3T)/T]^2}\ (T=2\text{ns}). \quad (19)$$

At first, we simulate the dipole at different positions in Cartesian FDTD region truncated by two boundaries, with no inner objects. These results can be considered as reference values. Then place the anti-SS-UPML ball into the space, we can obtain another set of results. Actually, because the absorbing material is set on both sides of the observers, the reflection caused by the absorber will be overlapped. Relative errors at these three points can be calculated and are shown in Fig. 7. Due to the huge amount of original data in the period of simulation time, we sample every 100 points and plot in the figure. Obviously, the SS-UPML performs very well in absorbing, its error of each point is similar to the original UPML. Besides, there is another interesting phenomenon in the cubic region we should care about, that the errors at three points have tiny differences as the reflections caused by the corner, edge and face are different, while a same level is maintained in spherical region because of the perfect symmetry of SS-UPML. This is the fundamental guarantee for SS-UPML to simulate larger scale and complex structural scatters.

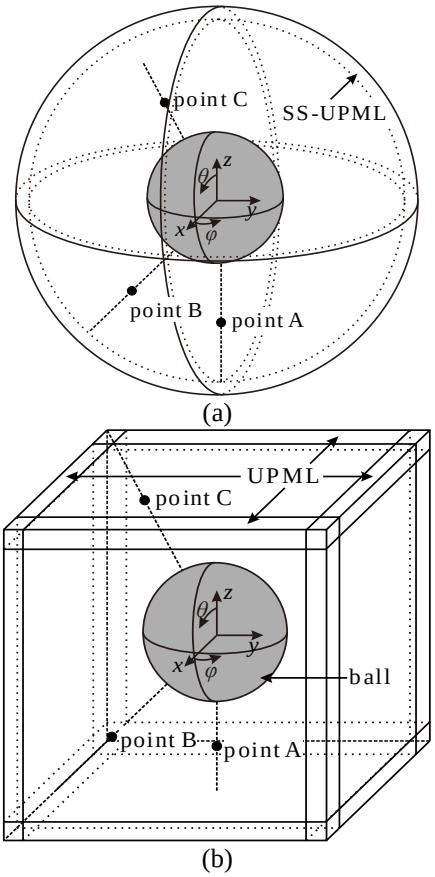

Fig. 6. Dipole in: (a) SS-UPML and (b) UPML truncated region with absorb object.

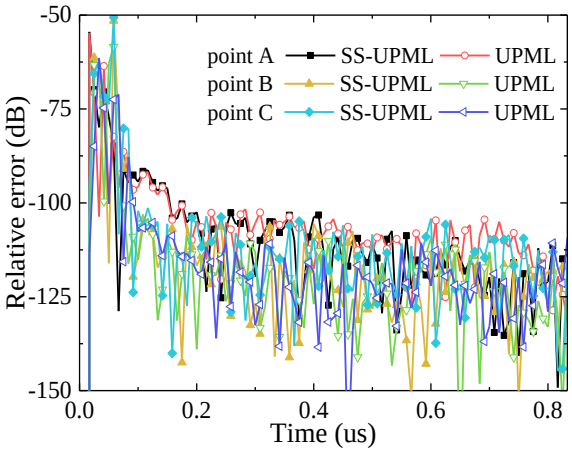

Fig. 7. Relative error of dipole radiation in different boundaries at different points.

B. Antenna simulation in SS-UPML

An inverted-F antenna is designed and calculated inside the SS-UPML. Its FDTD simulation result with different PMLs are presented and compared with finite element method (FEM). The structure and dimension of the antenna are shown in Fig. 8. The radiation element is designed on the top layer, and the ground is printed at the bottom layer. The plate thickness is 0.8mm, and has 2.2 dielectric constant. We use SS-UPML and UPML with 15 cells thickness as termination boundaries, and set at least 20 cells air gap in each direction between the antenna and the boundary. In this example, the FDTD problem space is composed of cells with 0.4mm in each direction. After we consider all these parts, the computational region is 161×161×161 in cubic boundary, and the radius of the spherical region is 161 cells, which makes the probability of 49.15% memory reduction.

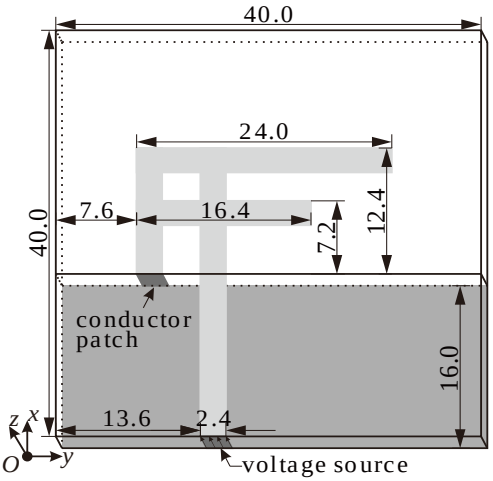

Fig. 8. Inverted-F antenna structure (unit: mm).

The antenna is excited by a voltage source, and its far-field frequencies are 2.4 and 5.8 GHz. The FDTD simulation of the antenna is performed with 7000 time steps, and a key parameter of the input port, return loss, is calculated. The results of S_{11} calculated by different algorithms are plotted in Fig. 9. Results of two FDTD boundaries show a good agreement with each other, and have a little difference to the FEM at low frequency domain, which is negligible effect on the final result. Most importantly, in the UPML boundary, 144.1MB memories are used and 1846.98s are cost for simulating the program. In our SS-UPML boundary, however, 76.7MB and 1067.65s are needed. This means 46.77% memory and 42.19% are saved, which coincide with the previous analysis, but keeps perfect accuracy.

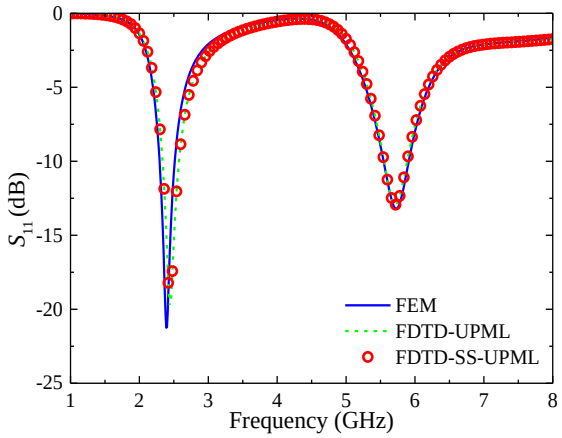

Fig. 9. Comparison of return loss calculated by different methods.

V. CONCLUSION

The SS-UPML strategy is applied for Cartesian FDTD in 3-D condition. We use this truncation boundary to calculate the different samples to test its performance. Due to the rotation of radial components in the Cartesian system, the equations in FDTD scheme can be simplified, which brings a huge convenience in programing. It reduces roughly half of the computational memory and time. In addition, it maintains high accuracy at different locations, even if the source is very close to the boundary. This is the foundation of future simulation for those objects with complex structures and material parameters. Our prospective study will pay much attention to appropriate parameters of SS-UPML for better absorbing performance, and more applications for 3-D cases.

ACKNOWLEDGMENT

This work is supported by the National Natural Science Foundation of China, under Grant 61671200, and the Key Project of Hebei Natural Science Foundation under grant F2017202283.

REFERENCES

[1] K. S. Yee, “Numerical solution of initial boundary

value problems involving Maxwell's equations in isotropic media," *IEEE Trans. Antennas Propag*., vol. 14, no. 3, pp. 302-307, 1966.

[2] Z. S. Sacks, D. M. Kingsland, R. Lee, and J. Lee. "A perfectly matched anisotropic absorber for use as an absorbing boundary condition," *IEEE Trans. Antennas Propag*., vol. 43, no. 12, pp. 1460-1463, 1995.

[3] S. D. Gedney, "An anisotropic perfectly matched layer absorbing media for the truncation of FDTD lattices," *IEEE Trans. Antennas Propag*., vol. 44, no. 12, pp. 1630-1639, 1996.

[4] W. C. Chew and W. H. Weedon, "A 3D perfectly matched medium from modified Maxwell's equations with stretched coordinates," *Microw. Opt. Technol. Lett*., vol. 7, no. 13, pp. 599-604, 1994.

[5] J. P. Bérenger, "A perfectly matched layer for the absorption of electromagnetic waves," *J. Comput. Phys*., vol. 114, no. 2, pp. 185-200, 1994.

[6] J. P. Bérenger, "Three-dimensional perfectly matched layer for the absorption of electromagnetic waves," *J. Comput. Phys*., vol. 127, no. 2, pp. 363-379, 1996.

[7] J. P. Bérenger, "Perfectly matched layer for the FDTD solution of wave-structure interaction problems," *IEEE Trans. Antennas Propag*., vol. 44, no. 1, pp. 110-117, 1996.

[8] N. V. Kantartzis, "Generalised higher-order FDTD-PML algorithm for enhanced analysis of 3D waveguiding EMC structures in cursvilinear coordinates," *IEE Proc.-Microw. Antennas Propag.*, vol. 150, no. 5, pp. 351-359, 2003.

[9] J. Wang, Z. Chen, J. Liang, Y. Wu, C. Peng, S. Tao, et al., "The split-field PML absorbing boundary condition for the unconditionally stable node-based LOD-RPIM method," *IEEE Antennas Wirel. Propag. Lett.*, vol. 17, no. 10, pp. 1920-1924, 2018.

[10] F. L. Teixeira, "On aspects of the physical reliability of perfectly matched absorbers for electromagnetic waves," *Radio Sci.*, vol. 38, no. 2, pp. 15-1-15-10, 2003.

[11] A. Taflove and S. C. Hagness, *Computational Electrodynamics*: *The Finite-Difference Time-Domain Method*. 3rd ed., Boston, USA: Artech House, 2005.

[12] A. Taflove, A. Oskooi, and S. G. Johnson, *Advances in FDTD Computational Electrodynamics*. Boston, USA: Artech House, 2013.

[13] J. F. Liu, Y. R. Pu, J. S. Zhang, and X. L. Xi, "An effective CFD-PML implementation for the cylindrical ADI-FDTD method," *IEEE Microw. Wirel. Compon. Lett.*, vol. 24, no. 12, pp. 824-826, 2014.

[14] W. Bao and F. L. Teixeira, "Performance analysis of perfectly matched layers applied to spherical FDTD grids," *IEEE Trans. Antennas Propag*., vol. 66, no. 2, pp. 1035-1039, 2018.

[15] A. P. Smull, A. B. Manić, S. B. Manić, and B. M. Notaroš, "Anisotropic locally conformal perfectly matched layer for higher order curvilinear finite-element modeling," *IEEE Trans. Antennas Propag*., vol. 65, no. 12, pp. 7157-7165, 2017.

[16] H. X. Zheng and K. W. Leung, "Radial perfectly matched layer for the ADI-FDTD method," *IEEE Microw. Wirel. Compon. Let*., vol. 19, no. 7, pp. 425-427, 2009.

[17] L. Wang, H. X. Zheng, M. J. Wang, and E. P. Li, "A circular-shaped perfectly matched layer strategy for rectangular FDTD grids," *Asia-Pacific Conference on Antennas and Propagation*, Xi'an, China, Oct. 2017.

[18] L. Wang and H. X. Zheng, "Circular-shaped uniaxial perfectly matched layer for the FDTD method in Cartesian system," *International Applied Computational Electromagnetics Society Symposium*, Beijing, China, July 2018.

[19] S. Dey and R. Mittra, "A locally conformal finite-difference time-domain (FDTD) algorithm for modeling three-dimensional perfectly conducting objects," *IEEE Microw. Guided Wave Lett*., vol. 7, no. 9, pp. 273-275, 1997.

Lu Wang received the B.S. and M.S. degrees from Tianjin University of Technology and Education, Tianjin, China, in 2014 and 2017, respectively. He currently works toward the Ph.D. degree in the Hebei University of Technology, Tianjin, China. His current research interest is computational electromagnetics, especially in the FDTD method. He has published more than 20 papers in refereed journals and conference proceedings. He received the Chinese National Scholarship in 2016 and participated in the Chinese Graduate Mathematical Contest in Modeling for three times since 2014 with national third prize.

Mengjun Wang was born in Hebei, China, in 1978. He received the B.S. in Information Engineering and M.S. in Physical Electronics from Hebei University of Technology, Tianjin China, in 1999 and 2005, respectively, and Ph.D. degree from Tianjin University, Tianjin, China, in 2008. He is working as an Associate Professor with School of Electronics and Information Engineering, Hebei University of Technology, Tianjin, China. His research

interests include microwave radio frequency technology, flexible electronics devices and electromagnetic compatibility.

Kanglong Zhang received the B.E. degree in Communication Engineering from Zheng-zhou University of Aeronautics, Zhengzhou, China, in 2016. He currently works toward his Ph.D. degree in Hebei University of Technology, Tianjin, China. His current research interest is computational electromagnetics, especially in the FDTD method.

Wenjie Cui received the B.S. degrees from Tianjin University of Technology and Education, Tianjin, China, in 2017. He currently works toward his M.S. degree in Hebei University of Technology, Tianjin, China. His current interest is the design and fabration of implantable medical antennas.

Hongxing Zheng received his Ph.D. degree in Electronic Engineering from Xidian University, Xi'an, in 2002. He is currently a Professor at School of Electronics and Information Engineering, Hebei University of Technology, Tianjin, China. He has authored six books and book chapters and more than 200 journal papers and 100 conference papers. He holds 40 China patents, issued in 2017. His recent research interests include wireless communication, design of microwave circuit and antenna, and computational electromagnetics.

Zheng is a Senior Member of the Chinese Institute of Electronics (CIE). He received the Young Scientists Award, in 2008, presented by the Tianjin Municipality, China.

Erping Li received the Ph.D. degree in Electrical Engineering from Sheffield Hallam University, Sheffield, U.K., in 1992. From 1993 to 1999, he was a Senior Research Fellow, Principal Research Engineer, Associate Professor, and the Technical Director at the Singapore Research Institute and Industry. In 2000, he joined the Singapore National Research Institute of High Performance Computing as a Principal Scientist and the Director of the Department of the Electronic and Photonics. He also holds the Distinguished Professor at Zhejiang University. He authored or coauthored more than 400 papers published in the referred international journals and conferences, authored two books. His research interests include electrical modeling and design of micro/nano-scale integrated circuits, 3-D electronic package integration, and nano-plasmonic technology.

Li is a Fellow of the MIT Electromagnetics Academy, USA. He has received numerous awards including the IEEE Electromagnetic Compatibility (EMC) Richard Stoddard Award for outstanding performance. He has served as an Associate Editor for number of IEEE Transactions and Letters. He has served as a General Chair and Technical Chair, for many international conferences. He was the founding General Chair for the 2008, 2010, and 2012 Asia-Pacific EMC Symposium. He has been invited to give numerous invited talks and plenary speeches at various international conferences and forums.